Experimental characterization of a commercial TEG device under mimicked operating conditions

# Experimental characterization of a commercial TEG device under mimicked operating conditions



IOP Publishing Nanotechnology
Nanotechnology 34 (2023) 085705 (11pp) https://doi.org/10.1088/1361-6528/aca20c

# Experimental characterization of a commercial TEG device under mimicked operating conditions

**Andrea Bottega[1], Elena Campagnoli[1], Claudio Dongiovanni[1] and Valter Giaretto[1,*]**

Department of Energy, Politecnico di Torino, Turin, Italy

E-mail: valter.giaretto@polito.it

Received 29 July 2022, revised 10 October 2022
Accepted for publication 11 November 2022
Published 12 December 2022

**Abstract**

A long-standing $zT = 1$ barrier is still present in commercial thermoelectric generator devices (TEG) and is typically not overcome. Although it is possible to accept the current limits of such devices, the performances reported on the datasheets are frequently not obtainable when these thermoelectric devices are arranged for use in the actual operating conditions. Despite this, the current primary energy prices and ongoing climate change make their use attractive for many industrial sectors. An experimental investigation is here proposed on a single type of TEG available on the market; the temperature relationships of the electrical resistivity, Seebeck coefficient, and thermal conductivity in a thermostatic chamber were first determined. A piece of apparatus was assembled to mimic the operating conditions of the TEG device and verify its performance, but some critical issues were highlighted regarding the heat transfer and its ability to maintain an adequate contact pressure on the hot and cold sides of the module. In order to extend the recovery of waste heat to a non-excessively high temperature in the hot forging process, the maximum temperature attained on the hot side of the TEG in the performed experiments was not allowed to exceed 180 °C. With temperatures of around 160 °C on the hot side and just over 40 °C on the cold side, the conversion efficiency was close to 3%. Considering this conversion efficiency and the operating conditions, the estimated order of magnitude of the electricity that could be produced by recovering heat waste in the Italian hot forging sector could be in the region of some hundreds of MWh per year.

Keywords: thermoelectric generator, semiconductor properties, TEG performance

(Some figures may appear in colour only in the online journal)

## 1. Introduction

In recent decades, research on thermoelectric materials has highlighted significant opportunities for improving their performance in the direct conversion of thermal energy into electricity. The dimensionless figure of merit $zT$ is a parameter that summarizes the thermoelectric performance of such materials and devices. This parameter compares electronic and thermal transport through a relationship between the power factor (which is dependent on the Seebeck coefficient and electrical resistivity at a given temperature) and thermal conductivity. It is expected that new thermoelectric materials, by using a nanostructuring techniques, or processing routes on the microstructure, will be able to overcome the current long-standing $zT = 1$ barrier, as reported in a large body of literature on the subject [1–10].

Despite the expectations regarding the performance of innovative materials, the current thermoelectric devices that are commonly available on the market are still assembled with non-optimized materials. Moreover, the volatility of the price of fossil fuels and the climate changes caused by their use have led to greater attention being paid to the efficiency of energy conversion processes.

* Author to whom any correspondence should be addressed.

 

Several applications of thermoelectric devices have proven to be advantageous for the recovery of thermal waste and its conversion into electrical energy over a wide range of temperatures. Typical examples are vehicle exhaust gases [11–14], the residual gases burned in the cementation process [15], and waste heat available at temperatures below 200 °C [16, 19]. Some applications of thermoelectric generators (TEGs) have also been proposed in the cogeneration field for the production of electricity and the recovery of heat from the cooling of devices for coalfield fires [17] and wood-fired stoves [18].

However, requests for the improvement of several processes in various industrial sectors are frequent, particularly for energy-intensive production. In this context, steel mills, and factories where metals are forged, tempered, and hardened, are of particular importance and attractive for thermoelectric generation. This manufacturing sector has a high energy budget, because of both the high thermal level required for processing (over 1200 °C) and the large quantities that are processed.

The Italian Hot Steel Forging Association (U.N.I.S.A., https://www.unisa.org/), which includes more than 60 companies, declared that about 0.9 million tons of steel have been processed in the last few years. After forging, the metal pieces are still at a high temperature (no lower than 1000 °C) and generally flow on a conveyor belt for the time necessary to reach an adequate thermal level before further processing or handling. Therefore, during cooling of the artifacts, it would be possible to collect heat and generate electricity using TEGs arranged along the conveyor belt.

A few applications aimed at thermoelectric generation from waste heat in steel mills and hot forging plants have been described in the literature [20, 21]. By employing thermoelectric devices based on bismuth telluride, the heat that has to be recovered, mainly due to thermal radiation of the hot manufactured material, is collected by a hot plate that supports the TEG devices. Similar operating conditions, in which the TEG systems face the casting slab [20] or the forged pieces at the maximum available thermal level [21] to obtain a temperature on the hot side of the TEGs as close as possible to the limit, which is approximately 330 °C for the employed modules, have been described. Different conversion efficiencies have been reported for these applications: over 7% in [20] and less than 3% in [21], for a comparable temperature difference between the hot and cold sides of TEGs.

Despite the appreciably different conversion efficiencies, these factory tests have confirmed there is a realistic opportunity for thermoelectric generation through the recovery of waste heat from the hot forging industry, as well as by adopting TEG devices characterized by classic thermoelectric materials [21]. Furthermore, these applications have been designed to exploit the highest thermal levels, although the optimal performance of thermoelectric materials based on $Bi_2Te_3$ alloys is typically found at lower temperatures [22].

Since the aforementioned temperature limit condition (330 °C) can only be reached in the initial part of the cooling process, it may be suitable to investigate the performance of these devices at lower temperatures in order to collect as much energy as possible from this process. In fact, according to the process indications provided by a company operating in the sector (Elind S.p.A., Venaria Reale, Turin), after forging, the largest hot pieces (up to a few liters in volume) are transported, on the conveyor belt, at a speed close to 1 m $min^{-1}$ for approximately ten meters before they reach a surface temperature below 400 °C.

On this basis, the aim of this study, which has adopted a different approach, is to extend the investigations described in the cited literature to lower temperatures on the hot side of TEG devices. For convenience, the TEG modules selected for testing (TEHP1–1994–1.5) are analogous to those used in [21], in terms of both materials and construction criteria.

The experiments were performed in a laboratory over successive stages. The first measurements stage was carried out in a thermostatic chamber to identify the dependence of the thermoelectric material properties on the temperature. The TEGs were tested at temperatures ranging from 10 °C to 180 °C. The temperature relationships were identified for the electrical resistivity, Seebeck coefficient, and thermal conductivity, using measurements that were performed over the specified range.

The second measurement stage, which was designed to simulate the operating conditions, was performed using a common electric stove as the heat source. Considering the limits of the heat source used on the hot side of the TEG, different test temperatures were chosen from the range investigated during the first measurement stage. A stable power supply from the source was used to maintain constant radiative emissions. Various thermal levels were obtained by modifying the view factor between the source and target with the aid of radiative shields.

In this phase, only one TEG module was studied, as described in the next section. The module was instrumented for the necessary thermal measurements (incoming heat flux and temperatures on both sides of the TEG), and the electrical measurements were performed under open- and closed-circuit conditions.

The performance curves of the TEG were determined experimentally by varying the electrical load and measuring the electrical current flowing in the circuit.

Comparisons between the measured and calculated performances are proposed in the Results and Discussion section according to the relationships that provide the temperature dependence of the thermoelectric properties.

## 2. Method and experimental arrangement

This section describes the experimental approach used to study the TEG devices. The goal was to characterize thermoelectric materials and devices under operating conditions at different temperatures. Therefore, both the considered equipment and experimental procedures are suitable for implementation in both laboratories and factories.

The materials and geometry of the devices are analyzed in section 2.1, the method used to determine the relationships that provide the temperature dependence of electrical, thermoelectric and thermal properties are explained in section 2.2, while the experimental arrangement and the methodology used to simulate the operating conditions are described in section 2.3.

**Table 1.** Thickness of the constituent materials.

| MATERIAL | | mm |
|---|---|---|
| HOT SIDE | Graphite sheet | 0.15 |
| | Alumina | 0.65 |
| | Conductive paste | 0.20 |
| | Copper | 0.35 |
| Legs height, $L$ | $Bi_2Te_3$ | 1.30 |
| Legs side, $w$ | | 1.30 |
| COLD SIDE | Copper | 0.35 |
| | Alumina | 0.65 |
| | Graphite sheet | 0.15 |

### 2.1. TEG materials

To determine the geometric dimensions of the constituent materials, only one TEG module was disassembled and the external layers and internal components, such as the semiconductor legs and electrical connectors, were measured.

Disassembly the TEG was relatively easy. In fact, after eliminating the silicone-based sealant positioned on the contour of one side of the module (the hot one, as indicated by the manufacturer), the ceramic plate was easily removed because it was simply 'glued' to the copper plates by a layer of a few tenths of a millimeter of conductive paste. Copper plates were firmly anchored to the ceramic substrate on the other side of the TEG.

Regarding the type of material used, the manufacturer only provided indications about the semiconductor legs, which were made of $Bi_2Te_3$. Some generic indications were provided for the contour plates (ceramic material, which we assumed were alumina) and for the external graphite plates deposited on both sides. No indications were given for the internal electrical connection, we assumed to be copper, or for the welding material. The latter was probably different for the hot and cold sides because of the different maximum temperatures allowed, 330 °C and 180 °C, respectively.

The total thickness (shoulder-to-shoulder) was measured for six TEG modules that were nominally equal in both dimensions and characteristics. All the thicknesses were found to be in the 3.75–3.85 mm range, with a mean average value of 3.80 mm. Each module had a plan size of area equal to 40 × 40 $mm^2$ and was composed of $N_P = 198$ thermoelectric pairs. The geometrical dimensions of the pillars and boundary layers were determined by selecting different parts of the disassembled TEG module.

The thermoelectric legs were cubic in shape, and the same thicknesses were assumed for the same material layers applied on both sides of the module. The fill factor of the module was evaluated as being close to 42%. The measured values in table 1 provide a stratigraphy of the thermoelectric module.

### 2.2. Thermostatic chamber investigations

The properties of the thermoelectric material were determined, as a function of temperature, by performing measurements in a thermostatic chamber at temperatures ranging from 10 °C to 180 °C. The apparatus and measurement methodology are those that have already been described in a previous work [23]; the arrangement and procedure detailed therein were adopted.

The figure pertaining to merit $z$ and ohmic series resistance $R$ of the tested thermoelectric modules were determined on the basis of the criterion suggested by Harman [24], using a commercial instrument (DX 4090) produced by RMT [29].

When determining the ohmic series resistance, the Harman method is not immune to the effect induced by the external thermal load at the $p - n$ junctions [27]. Therefore, the external graphite sheet was removed to reduce this effect from the TEG modules tested in the thermostatic chamber.

Three similar TEG modules, which were powered in sequence with electric current $I$ imposed by the DX 4090 instrument (typically in the 20–50 mA range) at each measurement temperature, were studied. The total Seebeck voltage $\Delta V_S$ produced at the junctions was measured as reported in [23]. A supply current of 25 mA was applied in all the tests to make the Joule effect negligible, according to the Harman method [24].

The temperature difference $\Delta T_J$ generated between the hot and cold junctions was determined by measuring the temperature difference, $\Delta T$, on the external surface of the ceramic layers (K-type thermocouples with exposed junctions made using 0.076 mm wires). Furthermore, a temperature correction, $\Delta_{Corr}$, was applied on both sides to take into account the total thermal resistance of the material layers surrounding the thermoelectric legs (see table 1)

$$\Delta T_j = \Delta T + \Delta_{Corr}. \tag{1}$$

The temperature correction was estimated by considering the TEG as a Peltier device fed with a constant current, thus the heat flux that affected the hot and cold sides of the module was evaluated. The low feeding current made the Joule effect negligible. For this reason, the Peltier and Fourier contributions were calculated using the values obtained from equations (5)–(7) for the properties of the thermoelectric materials, where $\Delta T_j = \Delta T$ was imposed. Further considerations about this correction are introduced in the Results and Discussion section.

The electrical and thermal properties of $p - n$ semiconductors cannot be determined separately by performing the measurements on an assembled module. In fact, the definition of the figure of merit $z$ ($K^{-1}$) of a thermoelectric module made of $N_P$ pairs is:

$$z = \frac{[N_P(S_p - S_n)]^2}{R\,K}, \tag{2}$$

where $S_p$ and $S_n$ are the Seebeck coefficients for legs $p$ and $n$, respectively, $R$ is the series electrical resistance and $K$ is the thermal conductance. In the case of $p$ and $n$ legs of the same length, $L$, and with the same cross section, $w^2$, $R$ and $K$ result to be:

$$R = N_P \frac{L}{w^2}(\rho_p + \rho_n);\ \ K = N_P \frac{w^2}{L}(\lambda_p + \lambda_n), \tag{3}$$

where $\rho_p$, $\rho_n$ and $\lambda_p$, $\lambda_n$ are the electrical resistivity and thermal conductivity of legs $p$ and $n$, respectively.

**Table 2.** Feeding current $I = 25$ mA: series resistance $R$, figure of merit $z$, Seebeck voltage $\Delta V_S$ and temperature difference at junctions $\Delta T_j$. The estimated uncertainty, c. l. 95% is in parentheses.

| $T$, °C | $R$, Ω | $z$, 1000 K$^{-1}$ | $\Delta V_S$, mV | $\Delta T_j$, K |
|---|---|---|---|---|
| 9.5 | 1.94 (0.05) | 1.47 (0.07) | 22.9 (0.7) | 0.42 (0.010) |
| 40.0 | 2.24 (0.08) | 1.7 (0.10) | 30.6 (0.8) | 0.53 (0.010) |
| 70.2 | 2.56 (0.07) | 1.92 (0.09) | 39 (1.1) | 0.63 (0.010) |
| 100.5 | 2.9 (0.10) | 2.1 (0.10) | 48 (1.3) | 0.73 (0.02) |
| 130.8 | 3.26 (0.08) | 2.1 (0.10) | 53.6 (0.8) | 0.80 (0.03) |
| 160.4 | 3.61 (0.09) | 2.0 (0.12) | 57 (1.0) | 0.83 (0.04) |
| 179.8 | 3.8 (0.12) | 1.8 (0.11) | 57 (1.2) | 0.83 (0.04) |

**Table 3.** Reference values $y_0$ of equation (8) at $T_0 = 25\ ^\circ C$ for $S$, ρ, λ and the temperature coefficients valid in the. 10 °C–180 °C temperature range.

| | $y_0$ | $b_1$, K$^{-1}$ | $b_2$, K$^{-2}$ |
|---|---|---|---|
| $S(T)$, μV K$^{-1}$ | 142.6 | $2.619{\cdot}10^{-3}$ | $-7.760{\cdot}10^{-6}$ |
| $\rho(T)$, μΩ m | 6.800 | $5.436{\cdot}10^{-3}$ | 0 |
| $\lambda(T)$, W m$^{-1}$ K$^{-1}$ | 1.871 | $-4.556{\cdot}10^{-3}$ | $15.08{\cdot}10^{-6}$ |

Therefore, by taking into account that $S_n$ is expected to be negative, the figure of merit can be rewritten as:

$$z = \frac{(S_p + |S_n|)^2}{(\rho_p + \rho_n)(\lambda_p + \lambda_n)}. \tag{4}$$

Depending on the doping elements, the properties of the $p$ and $n$ materials are generally different and only similar in some cases [25, 26]. Since the measured quantities in the proposed analysis are $R$ and $z$, the obtained properties are equivalent to those of the thermoelectric pair. When attributing properties to thermoelectric materials, it is just the same whether the same value is assumed for $p$ and $n$ or the average value is assumed for the pair. In both cases, the properties are the reference ones for both legs, which are useful for comparing different modules.

The electrical resistivity $\rho$, the Seebeck coefficient $S$, and the thermal conductivity $\lambda$ were determined at different temperatures, by means of equations (5)–(7)

$$\rho(T) = R\frac{w^2}{2N_P L} \tag{5}$$

$$S(T) = \frac{\Delta V_S}{2N_P \Delta T_J} \tag{6}$$

$$\lambda(T) = \frac{S^2}{\rho\, z}. \tag{7}$$

Table 2 shows, for the different imposed temperatures $T$, the mean values and estimated uncertainties for measured quantities $R$, $z$, $\Delta V_S$ and $\Delta T_J$.

The relationship chosen for the temperature dependence of the generic property, $y(T)$, obtained using equations (4)–(7), is:

$$y(T) = y_0[1 + b_1(T - T_0) + b_2(T - T_0)^2]\,, \tag{8}$$

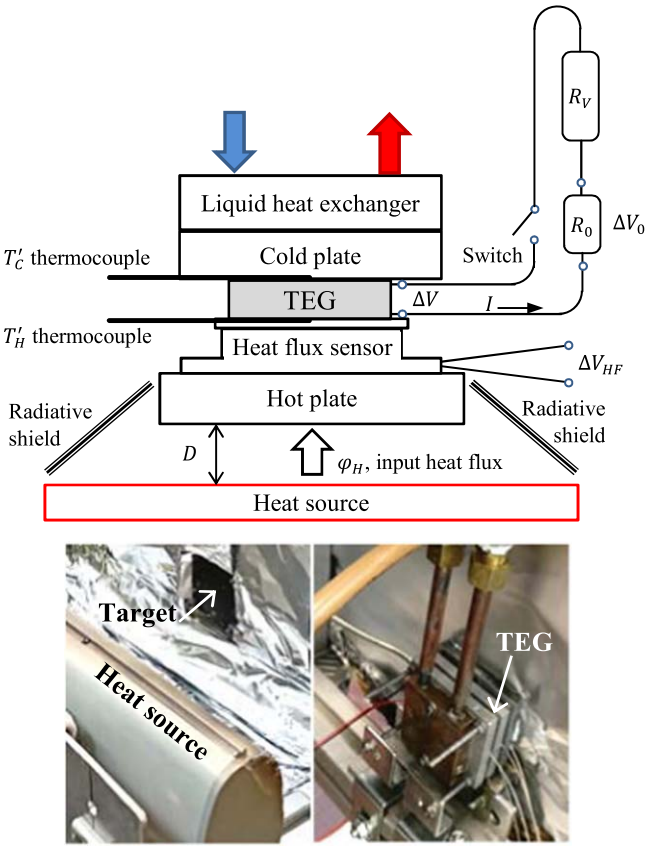


**Figure 1.** Sketch and pictures (front and back sides) of the experimental arrangement.

where $y_0$ is a property taken at the chosen reference temperature $T_0$. Table 3 reports the $S_0$, $\rho_0$ and $\lambda_0$ values at reference temperature $T_0$, as well as the first- and second-order temperature coefficients $b_1$ and $b_2$.

### *2.3. Characterization under mimicked operating conditions*

In order to determine the performance of the thermoelectric generators chosen in a temperature range that allows the opportunity for heat recovery and conversion to be extended, a TEG was characterized under mimicked operating conditions. In fact, considering the actual operating context for the case of hot forging, the thermal levels for heat recovery vary over a wide range of temperatures (but this is also the case for many other industrial sectors). Therefore, the average temperature value on the hot side of the TEG device is expected to be far from the temperature limit indicated by the manufacturer.

Figure 1 shows a sketch of the experimental arrangement, which includes the heat source that mimics the heat release by hot pieces and the TEG system used to manage and measure the thermal input quantities and electrical outputs.

Only one TEG module was used for the tests. It was assembled as supplied by the manufacturer, that is, covered by graphite sheets and, as suggested in the installation guide, clamped with two screws, where a tightening torque per screw of 1.25 Nm was applied.

The hot and cold plates were made of aluminum of the same thickness (8 mm each). The hot plate had a rectangular frontal area of 70 × 100 mm$^2$, which faced the hot source on one side and the heat flux sensor on the other (Hukseflux HIF01, calibrated by the manufacturer up to 900 °C). This sensor is made by a thermopile; therefore, the thermal flux is deduced from the voltage measured across the ends ($\Delta V_{HF}$ in figure 1).

The side of the hot plate facing the hot source represents the target surface and it was treated with special high-emissivity paint. On the other hand, the cold plate forms the interface for a liquid heat exchanger built entirely of copper, which uses water as the refrigerant fluid.

Two K-type sheathed thermocouples (1 mm in diameter) were placed in contact with the hot and cold sides of the TEG and housed in machined grooves on the surface of the cold plate and on an aluminum plate placed between the TEG and the heat flux sensor. The measured temperatures are indicated as $T_C'$ and $T_H'$ in figure 1 and are related to the junction temperatures $T_C$ and $T_H$, as explained in the results and discussion section.

The heat source was simulated using an electric stove with three hot elements that were 250 mm long, approximately 8 mm in diameter, and inserted into a forward-reflecting half-cavity. The maximum temperature of the hot elements was determined, using an infrared camera (Nippon Avionics InfReC R550), to be close to 745 °C and quite uniform in the axial direction. In order to exert a greater influence on the radiative exchanges than on the convective ones, the source and target surface of the hot plate were positioned vertically, facing each other at a relative distance $D$, as shown in figure 1. Since the radiative view factors between the source, target surface and surrounding environment influence the operating temperature on the hot side of the TEG to a great extent, the latter was adjusted by modifying the relative distance D and by means of radiative shields at the boundary.

Figure 1 shows the external electrical circuit connected to the TEG. The measured voltage drop, $\Delta V_0$, across calibrated resistance, $R_0$, allows an indirect measurement to be made of the generated electrical current. Variable resistance $R_V$ adjusts the electrical load of the circuit. The voltage drop, $\Delta V$, at the ends of the TEG lead wires was measured under open- and closed-circuit conditions. When the switch of the external electrical circuit ($I = 0$) was turned off, the measured voltage coincided with the Seebeck voltage $\Delta V_S$

$$\Delta V \equiv \Delta V_S = 2N_P \widetilde{S}\,(T_H - T_C), \tag{9}$$

where $\tilde{\varepsilon}$ is the effective Seebeck coefficient, defined as

$$\tilde{S} = \frac{1}{(T_H - T_C)} \int_{T_C}^{T_H} S(T)dT, \tag{10}$$

therefore

$$\Delta V \equiv \Delta V_S = 2N_P \int_{T_C}^{T_H} S(T)dT. \tag{11}$$

Conversely, when the switch was turned on, the electrical current flew in the circuit, and the measured voltage $\Delta V$ depended on the load resistance

$$R_L = R_V + R_0 = \frac{\Delta V}{I} = R_0 \frac{\Delta V}{\Delta V_0}, \tag{12}$$

but also on the Seebeck voltage and ohmic voltage drop, as a result of the effective series resistance $\tilde{R}$ of the thermoelectric legs

$$\Delta V = \Delta V_S - I\widetilde{R} = 2N_P \int_{T_C}^{T_H} S(T)dT - I\widetilde{R}, \tag{13}$$

where the effective series resistance is given by

$$\tilde{R} = \frac{2N_P}{(T_H - T_C)} \frac{L}{w^2} \int_{T_C}^{T_H} \rho(T)dT. \tag{14}$$

Moreover, the electric output power was computed as

$$W_e = I \cdot \Delta V = I\left(2N_P \int_{T_C}^{T_H} S(T)dT - I\tilde{R}\right). \tag{15}$$

## 3. Results and discussion

Three specimens of the chosen TEG module housed in the thermostatic chamber were analyzed at seven different temperatures, $T$, in the 10 °C–180 °C range. The three TEG modules were tested sequentially at each temperature $T$, after reaching the steady-state condition, by perturbing their equilibrium. By supplying a constant electric current (25 mA) for a given time interval (40 s), a stable temperature difference $\Delta T$ was observed between the two sides of the TEG, and the resulting Seebeck voltage $\Delta V_S$ was measured. After interrupting the power supply, the procedure was repeated, but this time reversing the polarity when the initial equilibrium was reached.

This measurement procedure was repeated twice for each module at the selected temperatures. An example of the temperature difference measured during the transient between the cold side and the hot sides (and vice versa) is shown in figure 2 for two tests: at the lowest temperature (∼10 °C, triangles) and at the highest (∼180 °C, circles). Open and solid markers indicate repeated measurements.

Since the same electric supply current was used for all the tests, the different temperature responses recorded for the TEG modules in figure 2 are clearly attributable to the temperature dependence on the properties of the thermoelectric materials, in particular, on the Seebeck coefficient and thermal conductivity.

The effective temperature difference between the junctions was obtained using equation (1) to evaluate the proper temperature correction. By assigning a typical thermal conductivity value of silicone-based compounds, about 4 W m$^{-1}$ K$^{-1}$, to the layer of conductive paste, and assigning the values found in the literature, based on what is reported in table 1, to the other layers, an average value of the overall thermal resistance of approximately 0.03 K W$^{-1}$ was estimated.

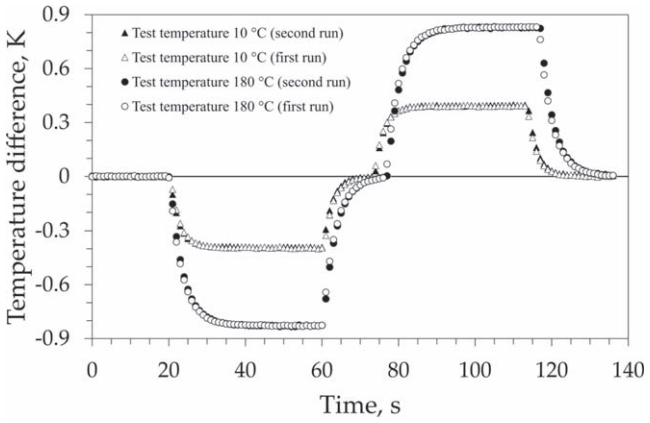


**Figure 2.** Temperature difference measured between the sides of a module versus time, in two subsequent runs and at different test temperatures.

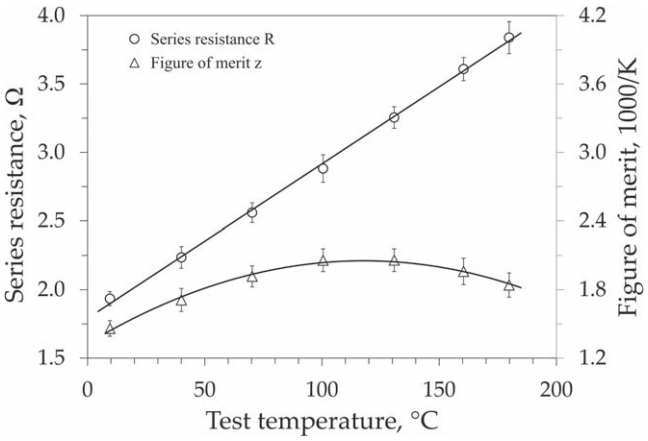


**Figure 3.** Measured values versus the temperature of series resistance $R$ and figure of merit $z$. The error bars are in agreement with the uncertainties shown in table 2. The continuous lines are the linear (series resistance) and the quadratic (figure of merit) trends.

The cold side is practically adiabatic (the Peltier effect compensates for Fourier heat conduction) for the adopted supply current (negligible Joule effect). Therefore, the total thermal power that affected the hot side was close to 1 W for each test, and a fairly constant temperature correction was obtained, the average value of which did not exceed 0.03 $K$.

The average values of the measured quantities in table 2, for each temperature, are: series resistance $R$, figure of merit $z$, Seebeck voltage $\Delta V_S$ and temperature difference of the junctions $\Delta T_j$. These mean values were determined by considering the spread between the values measured for the three TEG modules, and thus the uncertainties reported in parentheses, evaluated at a confidence level (c. l.) of 95%, were obtained.

The temperature dependence of the measured series resistance and the figure of merit are shown in figure 3. The markers represent the measured values, and the error bars are in agreement with the uncertainties reported in table 2, while the continuous lines are the linear and quadratic trends obtained for the series resistance and figure of merit, respectively.

The equivalent values for the properties of the thermoelectric material were obtained for each test temperature using the mean values in table 2 and equations (5)–(7). The coefficients that are valid for the general relationship in equation (8) were obtained by means of regression, with a correlation coefficient close to 0.999 for the three cases, and are reported in table 3.

The plots of these properties are shown in figure 4 as a function of the temperature, with error bars that are in accordance with the uncertainties reported in table 2.

In these figures, the gray bands between dashed lines indicate the values of these properties obtained by the authors in a previous investigation [23], performed on $Bi_2Te_3$ based Peltier modules of various manufacturers, and with characteristics in a temperature range of up to 90 °C.

The comparison shows similar trends with respect to the temperature, particularly for the electrical resistivity and thermal conductivity. The absolute values were also consistent with the previous ones for both of these properties. In fact, a low electrical resistivity corresponds to a high thermal conductivity (and vice versa), as expected for semiconductor materials classified as not optimized. The Seebeck coefficient values obtained for the semiconductors that characterized the analyzed TEG devices are the most surprising. As shown in figure 3(c), the comparison with previously obtained values showed an almost constant reduction of approximately 20%. This apparently resulted in an increase of around $5{\cdot}10^{19}$ $cm^{-3}$ of the carrier concentration on both of the p-n materials, as also reported in the literature [5] for $Bi_2Te_3$.

No evident reason emerges for this result from the measurements that were carried out and the procedure that was adopted. It is impossible to determine whether the unexpected value of the Seebeck coefficient is intrinsic to the semiconductors or conditioned by technological issues. In fact, the manufacturer indicated different limit temperatures for the hot and cold sides (330 °C and 180 °C, respectively), and the probably different welding materials employed to make the junctions on the hot and cold sides could have affected this coefficient.

The dimensionless figure of merit $zT$ (triangles) and power factor $S^2T/\rho$ (circles) are reported in figure 5. These synthetic parameters confirm the performance of traditional thermoelectric materials and indicate their optimal values as being approximately 150 °C.

Several operating temperatures were imposed on the hot side of the investigated TEG module, and the distance $D$ between the source and the target surface of the hot plate was modified, as shown in figure 1. By changing the distance $D$, the calculated view factor between the source and the target was changed over the 0.1–0.25 range.

In this investigation, the fundamental task was to determine the actual temperatures $T_H$ and $T_C$ of the hot and cold junctions, with the temperatures $T'_H$ and $T'_C$ measured on both sides of the TEG being known. Unlike the previous measurements carried out with the thermostatic chamber, the thermal power that affects the module was high, ranging from 30 to 150 W, and the thermal resistances on both sides of the

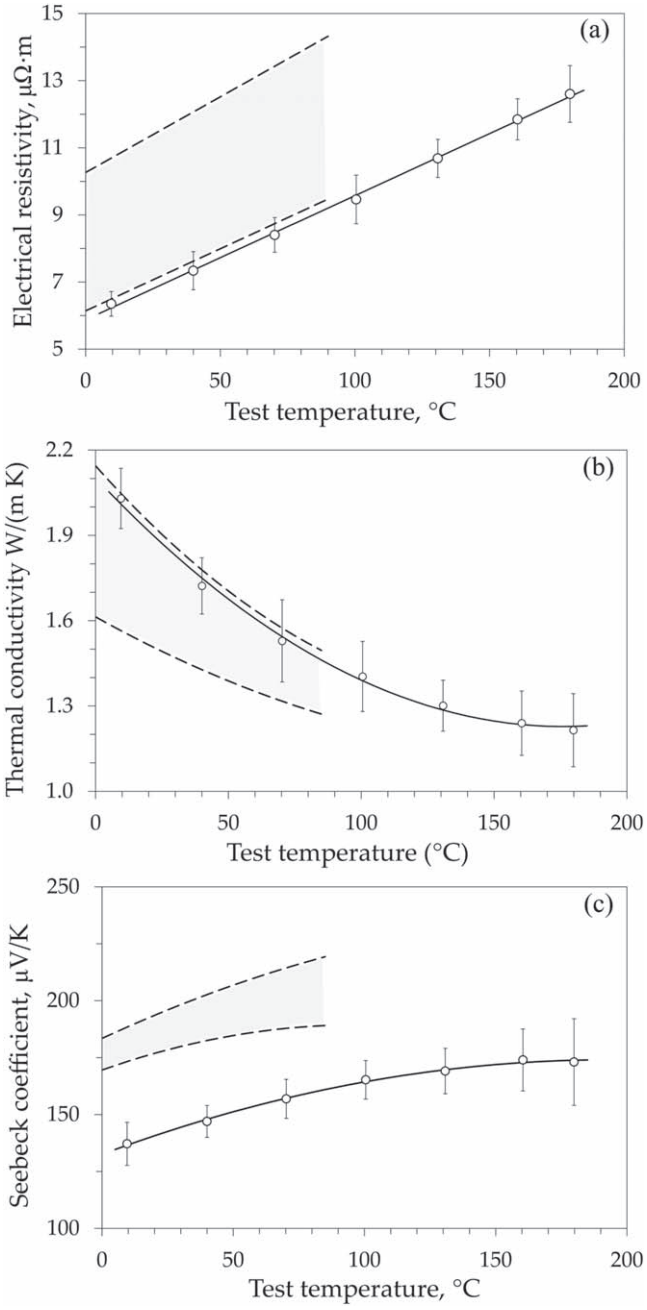


**Figure 4.** Determined properties of the semiconductors versus temperature: (a) electrical resistivity, (b) thermal conductivity, (c) Seebeck coefficient. Markers refer to the mean values and the error bars represent the uncertainties (c. l. 95%) . The grey bands refer to the values of the properties obtained up to 90 °C in previous experiments performed on $Bi_2Te_3$ based Peltier modules [23].

TEG produced significant differences from the temperatures mentioned above.

The thermal resistances $R_{t,H}$ and $R_{t,C}$ at the hot and cold interfaces were determined considering all the layers surrounding the junctions, as reported in table 1, and an equal thermal contact resistance between the plate that supported the sheathed thermocouple and the surface of the TEG on both sides. Moreover, a temperature coefficient for thermal contact resistance was introduced to account for possible reductions in the clamping force at different temperatures.

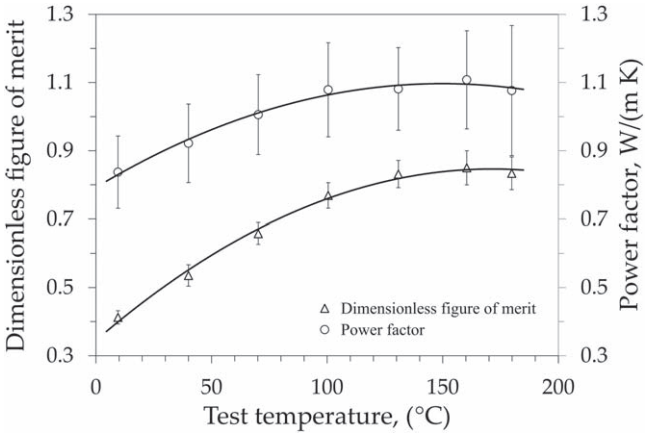


**Figure 5.** Dimensionless figure of merit $zT$ and the power factor $S^2T/\rho$ versus temperature. The error bars represent the uncertainties (c. l. 95%).

**Table 4.** Measured quantities in open circuit conditions: $T'_H$, $T'_C$, $\varphi_H$ and $\Delta V_S$. The junction temperatures $T_H$ and $T_C$ were calculated with equation (16).

| $T'_H$, °C | $T'_C$, °C | $\varphi_H$, W cm$^{-2}$ | $\Delta V_S$, V | $T_H$, °C | $T_C$, °C |
|---|---|---|---|---|---|
| 32.6 | 19.4 | 0.930 | 0.569 | 30.8 | 20.7 |
| 37.4 | 19.9 | 1.218 | 0.759 | 35.0 | 21.6 |
| 44.1 | 20.8 | 1.604 | 1.016 | 40.8 | 23.0 |
| 50.9 | 20.4 | 2.075 | 1.336 | 46.5 | 23.3 |
| 61.8 | 21.5 | 2.717 | 1.786 | 55.9 | 25.3 |
| 88.1 | 24.4 | 4.211 | 2.900 | 78.1 | 30.3 |
| 130.6 | 31.4 | 5.765 | 4.666 | 115.0 | 39.8 |
| 136.3 | 34.0 | 6.199 | 4.861 | 119.2 | 43.1 |
| 145.7 | 29.5 | 6.573 | 5.493 | 127.2 | 39.0 |
| 162.1 | 31.9 | 7.536 | 6.197 | 139.9 | 42.9 |
| 192.5 | 35.9 | 8.935 | 7.561 | 164.1 | 49.2 |

Considering the measured incoming heat flux $\varphi_H$ and these thermal resistances, and assuming that there are no heat losses on the lateral surfaces of the TEG at a steady state, the temperatures $T_H$ and $T_C$ of the hot and cold junctions can be obtained from the measured temperatures $T'_H$ and $T'_C$ as

$$T_H = T'_H - R_{t,H}\varphi_H, \;\; T_C = T'_C + R_{t,C}\varphi_H. \tag{16}$$

The first set of measurements was performed under open circuit conditions ($I = 0$). Thus, the voltage drop at the end of the TEG leads was only due to the Seebeck effect.

Considering the relationship defined for coefficient $S(T)$, the Seebeck voltage can also be calculated using equation (11). Therefore, the best agreement between the measured and calculated Seebeck voltages can be obtained by assigning an appropriate value to the temperature coefficient of the thermal contact resistance.

Table 4 lists the measured quantities and junction temperatures calculated using equation (13), while figure 6 shows a comparison of the measured and calculated Seebeck voltages. In this figure, the cross markers indicate the calculated Seebeck voltage when the thermal resistances $R_{t,H}$ and $R_{t,C}$

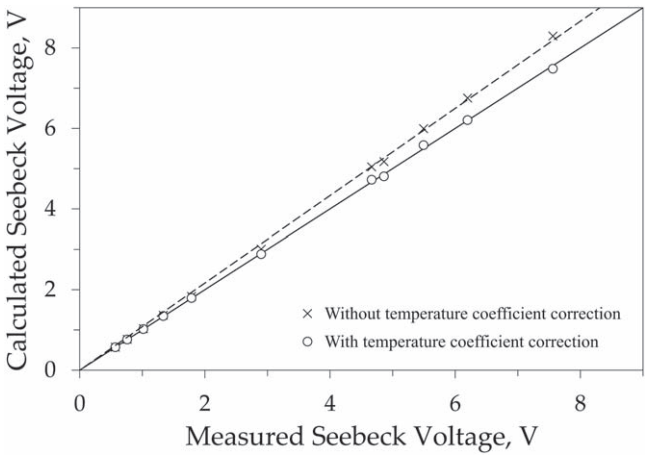


**Figure 6.** Comparison between the measured and the calculated Seebeck voltage. The cross markers refer to a zero temperature coefficient for the thermal contact resistance. The circle markers refer to a correction of the thermal contact resistance with a temperature coefficient of $8.5{\cdot}10^{-3}$ $K^{-1}$.

are assumed to be constant in temperature (zero temperature coefficient for the thermal contact resistance), while the circle markers refer to a correction of the thermal contact resistance with a temperature coefficient of $8.5{\cdot}10^{-3}$ $K^{-1}$.

From an electrical point of view, the Seebeck voltage represents the driving force that could be capable of overcoming the series resistance of the semiconductors and the external resistance of the load by producing an electric current in the circuit. Therefore, the possibility of determining the Seebeck voltage and series resistance of semiconductor materials, as a function of the temperature of the junctions, allows the performance of the TEG device to be identified.

Given the junction temperatures, equation (13) produces a linear trend in a voltage–current diagram, whose negative slope coincides with the series resistance of the semiconductors, while the intercept corresponds to the Seebeck voltage. The ratio between the Seebeck voltage and semiconductor series resistance sets the limit current. Thus, by varying the current to this limit value, using equation (12), the output power curve can be obtained, for which the matched load resistance is that of a semiconductor series.

Some thermal scenarios were reproduced in a similar manner to the previous ones to obtain a complete experimental characterization of the TEG device, but in this case the switch was turned on to power the load with the generated electric current.

The performance of the TEG module was determined by measuring current $I$ for various electrical loads and assigning different values to resistance $R_V$ (figure 1). The measurements conducted under these conditions gave a new set of values for the input heat flux, interface temperatures on both sides of the TEG, voltage difference at the potential leads, and new values for the temperatures of the junctions. The latter were obtained using thermal resistances, $R_{t,H}$ and $R_{t,C}$, that had previously been calibrated in temperature and considering that the heat flux involving the cold side of the TEG, in this case, was reduced because of the generated electrical power.

**Table 5.** Some thermal and electric quantities determined for the operating conditions. $\Phi_H$, $T_H$ and $T_C$ are the mean values obtained for the various imposed load resistances. $\Delta V_S$ is the Seebeck voltage determined with equation (11), using the coefficients in table 3, and the junction temperatures $T_H$, $T_C$. $R_L$, and $W_e$ are the matched load resistance and electric power output, respectively. $\eta = W_e/\Phi_H$ is the conversion efficiency.

| $\Phi_H$, W | $T_H$, °C | $T_C$, °C | $\Delta V_S$, V | $R_L$, Ω | $W_e$, W | $\eta$, % |
|---|---|---|---|---|---|---|
| 33.2 | 48.9 | 25.0 | 1.390 | 2.72 | 0.18 | 0.5 |
| 87.1 | 100.5 | 34.5 | 4.077 | 3.17 | 1.31 | 1.5 |
| 110.8 | 121.5 | 40.5 | 5.122 | 3.09 | 2.12 | 1.9 |
| 148.5 | 156.9 | 43.9 | 7.459 | 3.39 | 4.10 | 2.8 |

Some thermal and electric quantities determined for the operating conditions are listed in table 5. The input heat power and junction temperatures are the mean values obtained for various imposed load resistances (3% is the maximum spread). The Seebeck voltages $\Delta V_S$ in table 5 were determined using equation (11), with the coefficients listed in table 3, and the junction temperatures. Both the matched load resistances and the output electric powers were obtained under the mimicked operating conditions. The conversion efficiency $\eta = W_e/\Phi_H$, whose maximum obtained value is 2.8%, is also shown in the table.

The complete set of experimental results is shown in figures (7) and (8). The open markers refer to the measurements, whereas the solid ones represent the Seebeck voltages calculated as explained above. These values are in good agreement with those obtained by extrapolating the linear trend that represents the measurements, as indicated by the continuous lines in figure 7, whose slope corresponds, with a negative sign, to the matched load resistances $R_L$ shown in table 5.

Since the matched value of the load resistance is expected to be in agreement with the series resistance of the legs ($R_L \equiv \tilde{R}$), the latter can be determined using equation (14), on the basis of the $T_H$ and $T_C$ values in table 5, and defining the voltage–current trends shown in figure 7 with dashed lines through equation (13). These voltage–current trends show different slopes, with a deviation that exceeds 10%.

A similar behavior is shown in figure 8, which reports the electric power output measured as a function of the electric current (open marker). In this diagram, the solid lines were obtained by considering the measured matched load resistance $R_L$, while the dashed ones were determined using equation (12), with the series resistance $\tilde{R}$ of the legs and the Seebeck coefficient obtained from measurements performed in a thermostatic chamber.

A comparison with the investigation carried out in the thermostatic chamber shows that the electrical properties of the TEG device worsen under the operating conditions, regardless of the temperatures at the junctions. To explain this lower performance, it should be considered that, in addition to the measurement uncertainties (in particular for the geometric dimensions of the semiconductors), it cannot be ruled out that

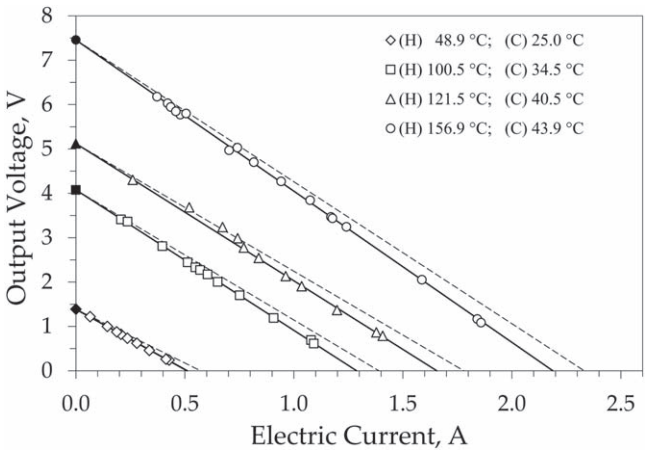


**Figure 7.** Output voltage versus current for the different operating conditions summarized in table 5. The solid markers represent the measured Seebeck voltage. The continuous lines were obtained by means of regression on the values measured under the operating conditions (open markers), while the dashed lines represent the expected trend, considering the properties of the semiconductors obtained through investigations in a thermostatic chamber and the effective series resistance given by equation (14). Symbols (H) and (C) stand for hot and cold side respectively.

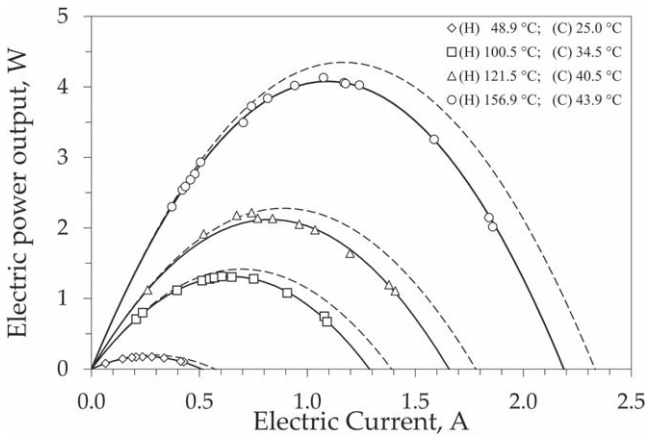


**Figure 8.** Electric power output versus current for the different operating conditions summarized in table 5. The continuous lines were obtained by means of regression of the values measured under the operating conditions (open markers), while the dashed curves represent the expected trend, considering the properties of the semiconductor obtained from investigations in a thermostatic chamber and the power output given by equation (15). Symbols (H) and (C) stand for hot and cold side respectively.

the imposition of the tightening torque had modified the electrical connections inside the device.

The authors believe, on the basis of the results presented in table 5 and with reference to the performance determined in operating conditions, that thermal energy recoveries that produce lower temperatures than 100 °C at the hot side could be inappropriate, because of the low conversion efficiency. Conversely, with temperatures on the hot side of around 160 °C and just over 40 °C on the cold side, the conversion efficiency was found to be close to 3%. This result does not agree with the indications reported in the datasheet supplied by the manufacturer for the same temperature range. However, the same conversion efficiency found in this investigation has also been obtained by other authors [21] who carried out measurements on similar devices under apparently higher temperatures on the hot side of the TEGs.

The measured dimensionless figure of merit close to one and the determined power factor lower than one, as shown in figure 5, indicate that the investigated TEGs are not evolved in terms of performance. If the heat recovery and conversion into electrical energy are carried out from thermal waste, these two performance parameters retain their importance, but the density of the produced electrical power could be the real discriminating parameter to achieve economic feasibility [28]. In the studied case, the maximum power density was obtained at around 2.5 kW $m^{-2}$, and an investment aimed solely at electricity production may therefore not be sustainable.

Considering the production data declared by UNISA (https://www.unisa.org/), that is, of about 0.9 million tons of forged steel per year, their overall thermal capacity can be estimated as approximately 0.45 TJ $K^{-1}$.

If it is hypothesized that a quarter of the total heat wasted during the cooling of the pieces (from 1200 °C to 400 °C) could be recovered and if a conversion efficiency of 2.5% is assumed, the order of magnitude of the electricity that can be produced by TEGs can be estimated at some hundreds of MWh per year.

## 4. Conclusions

The main objective of this investigation has been to evaluate the performance of a thermoelectric generator, both by determining the temperature dependence of the properties and by reproducing the possible operating conditions. The identification of the relationship between the temperature, and the electrical, thermal, and thermoelectric properties, is a fundamental step toward justifying and verifying the performance of these devices under operating conditions.

Regardless of the maximum thermal levels allowed by the device, the investigation was carried out over a lower temperature range in order to propose further applications, even in contexts where the available thermal levels are not very high. This is an advantage for these devices, and we believe it is an important aspect for proposing effective applications for large industrial sectors, possibly with a minimum impact on the production cycle, in part due to their small size.

Under these operating conditions, predictable problems, such as those associated with heat transfer from the source to the device, were encountered. In addition, the assembly of the recovery and conversion system highlighted certain critical issues, particularly regarding the choice of the proper value of the contact pressure at the interfaces and its preservation when the operating temperature varied. These critical aspects should be appropriately considered for the correct design of recovery systems.

The reliability of thermoelectric devices is commonly considered somewhat high. Even in the absence of a durability test protocol for the classification of commercial

devices, their intrinsic simplicity and the absence of moving parts, as a first approximation, make their physical duration coincide with or greater than the economic life of the system in which they are applied.

The current low efficiency of commercial devices (typically less than 3.5% [21]) is certainly one of the major limits for industrial applications. Considering that a low electrical conversion efficiency corresponds to a large amount of heat discarded on the cold side of the TEGs, by properly choosing the temperature of the cold side, the amount of heat not converted into electrical energy could be used, for example, for space heating, thus making the application of thermoelectric devices particularly attractive for this industrial sector.

## Acknowledgments

The authors would like to thank Mr M Bressan and Mr R Costantino for their helpful support in realizing the experimental setup.

## Data availability statement

All data that support the findings of this study are included within the article (and any supplementary files).

## Funding statement

The study was supported by the Department of Energy, at the Politecnico di Torino.

## Ethical compliance

All the procedures performed in studies involving human participants were conducted in accordance with the ethical standards of the institutional and/or national research committee and according to the 1964 Helsinki Declaration and its later amendments or comparable ethical standards.

## Conflict of interest declaration

The authors declare that they have NO affiliations with or involvement in any organization or entity with any financial interest in the subject matter or materials discussed in this manuscript.

## ORCID iDs

Andrea Bottega https://orcid.org/0000-0002-1111-0796
Elena Campagnoli https://orcid.org/0000-0003-3000-8065
Claudio Dongiovanni https://orcid.org/0000-0002-0786-2784
Valter Giaretto https://orcid.org/0000-0003-2243-7791

## References

[1] Neophytou N, Zianni X, Kosina H, Frabboni S, Lorenzi B and Narducci D 2013 Simultaneous increase in electrical conductivity and seebeck coefficient in highly boron-doped nanocrystalline Si *Nanotechnology* **24** 205402
[2] Dehkordi A M, Zebarjadi M, He J and Tritt T M 2015 Thermoelectric power factor: Enhancement mechanisms and strategies for higher performance thermoelectric materials *Mater. Sci. Eng. R Rep.* **97** 1–22
[3] Hao F, Xing T, Qiu P, Hu P, Wei T, Ren D, Shi X and Chen L 2018 Enhanced thermoelectric performance in n-type $Bi_2Te_3$-based alloys via suppressing intrinsic excitation *ACS Appl. Mater. Interfaces* **10** 21372–80
[4] Chen Z, Zhang X and Pei Y 2018 Manipulation of Phonon Transport in Thermoelectrics *Adv. Mater.* **30** 1705617
[5] Witting I T, Chasapis T C, Ricci F, Peters M, Heinz N A, Hautier G and Snyder G J 2019 The Thermoelectric Properties of Bismuth Telluride *Adv. Electron. Mater.* **5** 1800904
[6] Cha J, Zhou C, Cho S P, Park S H and Chung I 2019 Ultrahigh power factor and electron mobility in n-Type $Bi_2Te_3$–x%Cu stabilized under excess Te condition *ACS Appl. Mater. Interfaces* **11** 30999–1008
[7] Hanus R, Agne M T, Rettie A J E, Chen Z, Tan G, Chung D Y, Kanatzidis M G, Pei Y, Voorhees P W and Snyder G J 2019 Lattice softening significantly reduces thermal conductivity and leads to high thermoelectric efficiency *Adv. Mater.* **31** 1900108
[8] Zhang D, Cao Y, Hui Y, Cai J, Ji J, Yin H, Zhang M, Xu J and Zhang Q 2022 Enhancements of thermoelectric performance in n-type $Bi_2Te_3$-based nanocomposites through incorporating 2D Mxenes *J. Eur. Ceram. Soc.* **42** 4587–93
[9] Artini C, Castellero A, Baricco M, Buscaglia M T and Carlini R Structure, microstructure and microhardness of rapidly solidified $Sm_y(Fe_xNi_{1-x})_4Sb_{12}$ (x = 0.45, 0.50, 0.70, 1) thermoelectric compounds 2018 *Solid State Sci.* **79** 71–8
[10] Aversano F, Branz S, Bassani E, Fanciulli C, Ferrario A, Boldrini S, Baricco M and Castellero A 2019 Effect of rapid solidification on the synthesis and thermoelectric properties of Yb-filled $Co_4Sb_{12}$ skutterudite *J. Alloys Compd.* **796** 33–41
[11] Saidur R, Rezaei M, Muzammil W K, Hassan M H, Paria S and Hasanuzzaman M 2012 Technologies to recover exhaust heat from internal combustion engines *Renew. Sustain. Energy Rev.* **16** 5649–59
[12] Durand T, Eggenschwiler P D, Tang Y, Liao Y and Landmann D 2018 Potential of energy recuperation in the exhaust gas of state of the art light duty vehicles with thermoelectric elements *Fuel* **224** 271–9
[13] Muralidhar N, Himabindu M and Ravikrishna R V 2018 Modeling of a hybrid electric heavy duty vehicle to assess energy recovery using a thermoelectric generator *Energy* **148** 1046–59
[14] Comamala M, Massaguer A, Massaguer E and Pujol T 2019 Validation of a fuel economy prediction method based on thermoelectric energy recovery for mid-size vehicles *Appl. Therm. Eng.* **153** 768–78
[15] Kaibe H, Makino K, Kajihara T, Fujimoto S and Hachiuma H 2012 Thermoelectric generating system attached to a carburizing furnace at komatsu ltd, awazu plant *Proc. of the 9th European Conf. on Thermoelectris AIP Conf. Proc.* 1449 (Thessaloniky) 524
[16] Remeli M F, Tan L, Date A, Singh B and Akbarzadeh A 2015 Simultaneous power generation and heat recovery using a heat pipe *Energy Convers. Manag.* **91** 110–9
[17] Deng J, Zhou F, Shi B, Torero J L, Qi H, Liu P, Ge S, Wang Z and Chen C 2020 Waste heat recovery, utilization and evaluation of coalfield fire applying heat pipe combined thermoelectric generator in Xinjiang, China *Energy* **207** 118303

[18] Sornek K, Filipowicz M, Zoładek M, Kot R and Mikrut M 2019 Comparative analysis of selected thermoelectric generators operating with wood-fired stove *Energy* **166** 1303–13
[19] Ando Junior O H, Calderon N H and Silva de Souza S 2018 Characterization of a thermoelectric generator (TEG) system for waste heat recovery *Energies* **11** 1555
[20] Kuroki T, Kabeya K, Makino K, Kajihara T, Kaibe A H, Hachiuma H, Matsuno H and Fujibayashi A 2014 Thermoelectric generation using waste heat in steel works *J. Electron. Mater.* **43** 2405–10
[21] Ebling D G, Krumm A, Pfeiffelmann B, Gottschald J, Bruchmann J, Benim A C, Adam M, Labs R, Herbertz R R and Stunz A 2016 Development of a system for thermoelectric heat recovery from stationary industrial processes *J. Electron. Mater.* **45** 3433–9
[22] Shi X, Chen L and Uher C 2016 Recent advances in high-performance bulk thermoelectric materials *Int. Mater. Rev.* **61** 379–415
[23] Giaretto V and Campagnoli E 2020 The elusive thomson effect in thermoelectric devices. experimental investigation from 363 K to 213 K on various peltier modules *Metals* **10** 291
[24] Harman T C 1958 Special techniques for measurement of thermoelectric properties *J. Appl. Phys.* **29** 1373
[25] Goldsmid H J 1958 The electrical conductivity and thermoelectric power of bismuth telluride *Proc. Phys. Soc.* **71** 633–46
[26] Goldsmid H J 1956 The thermal conductivity of bismuth telluride *Proc. Phys. Soc.* B **69** 203–9
[27] De Marchi A and Giaretto V 2011 An accurate new method to measure the dimensionless figure of merit of thermoelectric devices based on the complex impedance porcupine diagram *Rev. Sci. Instrum.* **82** 104904.1
[28] Weishu L, Qing J, Hee Seok K and Zhifeng R 2015 Current progress and future challenges in thermoelectric power generation: from materials to devices *Acta Mater.* **87** 357–76
[29] Gromov G, Kondratiev D, Rogov A and Yershova L 2001 *Easy-to-use Application and Theory. In Proc. of the 6th European Workshop on thermoelectricity of the European Thermoelectric Society, Freiburg im Breisgau,* pp 1–8